International Journal of Pharmaceutics 429 (2012) 38–45

Contents lists available at SciVerse ScienceDirect

International Journal of Pharmaceutics

journal homepage: www.elsevier.com/locate/ijpharm

Yellow coloration phenomena of incorporated indomethacin into folded sheet mesoporous materials

Shuichi Tanabe [1], Kenjirou Higashi [1], Makoto Umino, Waree Limwikrant, Keiji Yamamoto, Kunikazu Moribe *

Graduate School of Pharmaceutical Sciences, Chiba University, 1-8-1, Inohana, Chuo-ku, Chiba 260-8675, Japan

ARTICLE INFO

Article history:
Received 27 December 2011
Received in revised form 24 February 2012
Accepted 6 March 2012
Available online 15 March 2012

Keywords:
Coloration
Solid-state NMR
Differential scanning calorimetry
Powder X-ray diffractometry
Folded sheet mesoporous materials
Amorphous

ABSTRACT

Solid-state ^{13}C nuclear magnetic resonance (NMR) spectroscopy that included relaxation time measurement was utilized to evaluate the yellow coloration of evaporated samples (EVPs) of indomethacin (IMC) with commercially available folded sheet mesoporous materials (TMPS). Colorimetric analysis by visible light reflection spectroscopy clarified the color differences in each sample: deep yellow-colored melt-quenched amorphous IMC, a slightly yellow-colored EVP of TMPS-1.5 (pore size: 1.8 nm), and a yellow-colored EVP of TMPS-7 (pore size: 7.3 nm). The color of EVPs changed from yellow to white after washing with ethanol, indicating the reversible coloration without a chemical reaction. Powder X-ray diffractometry and differential scanning calorimetry demonstrated that the EVPs of TMPS-7 entrapped greater amounts of amorphous IMC into the mesopore than TMPS-1.5. The amount of amorphous IMC in the mesopores could affect the strength of yellow coloration. Solid-state ^{13}C NMR spectroscopy that included spin–lattice relaxation time (T_1) measurement revealed that the mobility of the aromatic rings of amorphous IMC in TMPS mesopores was higher than that in melt-quenched amorphous IMC. The difference in color between amorphous IMC in TMPS mesopores and melt-quenched amorphous IMC can be explained by their distinct intramolecular π-conjugation systems.

© 2012 Elsevier B.V. All rights reserved.

1. Introduction

Drug coloration phenomena sometimes occur during pharmaceutical processing. Drug coloration is mostly induced by chemical reactions between drugs and excipients, and their subsequent decomposition (Rhee et al., 2008). It is no wonder that colored formulations due to chemical reactions should be avoided because the product quality is lost. Changes in the molecular state of drugs due to intermolecular interaction with excipients could lead to sample coloration as well (Sheth et al., 2005; Braun et al., 2008). There are also the cases where color change of photochromic molecules was induced by its conformational difference (Siewertsen et al., 2009). From formulation development and quality control perspectives, such colored samples without degradation and impurities might be acceptable as formulations, although sample coloration is not desirable. Hence, it is important to understand the coloration mechanisms of drug formulation. There are many reports about coloration phenomena occurring in chemical and engineering organic materials such as solar cells and organic dyes (Morimoto et al., 2003; Shen et al., 2009). However, most studies about coloration in the pharmaceutical field are limited to the quality control measures such as the quantitation of drug decomposition and validation (Siddiqui and Nazzal, 2007; Rhee et al., 2008). Few reports focus on the coloration phenomena of pharmaceutical compounds induced by change in molecular state and not by chemical reactions.

Coloration mechanisms are divided into two types: visible light absorption and visible light emission. For both mechanisms, the coloration of organic compounds depends on the electrical situation, such as the length of π-conjugated systems and/or electric delocalization from molecular structures, crystal structures, and molecular interactions (Braun et al., 2008; Yamamura et al., 2008; Siewertsen et al., 2009). It is necessary to obtain detailed, molecular-level information to analyze coloration phenomena in organic compounds effectively. Single-crystal X-ray analysis is considered the most useful method, although it cannot be applied for powder samples or pharmaceutical formulations, including drugs and excipients. Complementary analytical technologies for drug formulations such as powders, including X-ray diffraction, thermal analysis, solid-state fluorescence, and infrared measurements, can be used to investigate coloration phenomena. In particular, solid-state nuclear magnetic resonance (NMR) spectroscopy including relaxation time measurement, which can assess the atomic-level chemical environment and dynamics, is a powerful technique (Tishmack et al.,

* Corresponding author. Tel.: +81 43 226 2866; fax: +81 43 226 2867.
E-mail address: moribe@p.chiba-u.ac.jp (K. Moribe).
[1] These authors contributed equally to this study.

0378-5173/$ – see front matter © 2012 Elsevier B.V. All rights reserved.
doi:10.1016/j.ijpharm.2012.03.011

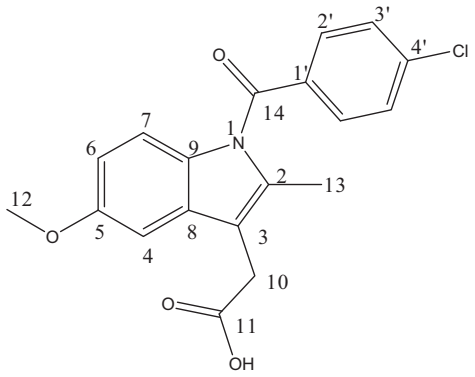

Fig. 1. Chemical structure of indomethacin (IMC).

2003; Geppi et al., 2008; Lubach et al., 2007). Sheth et al. (2005) used solid-state NMR techniques to demonstrate that the yellow coloration phenomenon of piroxicam is due to proton transfer.

Mesoporous silica is a porous honeycomb-like structure with a large specific surface area and highly controlled pore size. Recently, mesoporous materials have been proposed as host materials for improving drug properties such as dissolution and stability (Ambrogi et al., 2007; Mellaerts et al., 2008). We previously reported that various active pharmaceutical ingredients (APIs) (e.g., benzoic acid, salicylamide, flurbiprofen, prednisolone, and mefenamic acid) could be incorporated into the pores of mesoporous silica (Tozuka et al., 2003, 2005a,b; Nishiwaki et al., 2009; Moribe et al., 2010). Some APIs changed from white to colored after the incorporation process. Moribe et al. (2010) investigated the molecular state of mefenamic acid in colored samples using solid-state NMR and reported that changes in the molecular state of mefenamic acid in the pore could affect blue coloration. Reversible coloration is observed when *p*-nitroaniline is incorporated into the pores of ZSM-5, a kind of zeolite (Komori and Hayashi, 2003, 2004). Coloration as a result of the intermolecular interaction between *p*-nitroaniline and Na^+ of ZSM-5 is affected by water adsorption/desorption. However, the direct relationship between reversible coloration and the molecular state of pharmaceutical compounds is unclear.

In this study, we investigated the mechanism of yellow coloration in evaporated indomethacin/commercially available folded sheet mesoporous materials (TMPS). Various analytical techniques, including colorimetric analysis, powder X-ray diffractometry, differential scanning calorimetry, and solid-state NMR spectroscopy (including relaxation time measurements) were utilized to evaluate the coloration mechanism both quantitatively and qualitatively.

2. Materials and methods

2.1. Materials

The γ-form of indomethacin (IMC, 1-(*ρ*-chlorobenzoyl)-5-methoxy-2-methylindole-3-acetic acid) was purchased from Wako Pure Chemical Industries, Ltd. (Osaka, Japan). The chemical structure of IMC is illustrated in Fig. 1. IMC has two major polymorphs: the stable γ-form and metastable α-form. The α-form of IMC was obtained using a recrystallization method: a solution of 2 g of IMC in 7 mL of ethanol at 70 °C was rapidly cooled to 4 °C and stored overnight at 4 °C. The precipitated α-form crystals were collected by filtration and dried in vacuo at 40 °C (Masuda et al., 2006). Melt-quenched amorphous IMC was prepared by melting indomethacin at 165 °C and cooling it using liquid nitrogen (Savolainen et al., 2007). Taiyo Kagaku Co., Ltd. (Mie, Japan) kindly supplied TMPS-1.5 and TMPS-7. The mean pore sizes, specific surface areas, and pore volumes of TMPS-1.5 and TMPS-7 were 18 and 73 Å, 1019 and 826 m^2/g, and 0.37 and 1.1 cm^3/g, respectively. The TMPS was ground by mortar and pestle, sieved using a 125-μm sieve, and dried at 120 °C for 3 h in vacuo before use. All other chemicals were of reagent grade.

2.2. Sample preparation

The TMPS and γ-IMC were mixed at weight ratios of 7/3 and 5/5 in a glass vial for 1 min to obtain a physical mixture (PM). The TMPS was dispersed in an ethanol solution containing IMC. Weight ratios of IMC to TMPS in the suspension were 3/7 and 5/5. Then, the solution was sonicated for 3 min and evaporated at 30 °C. The resultant powder was dried at 60 °C for 24 h to obtain an evaporated sample (EVP). The EVP was dispersed in ethanol and sonicated for 10 min. The powder was filtrated and dried at 30 °C for 30 min to obtain washed EVP.

2.3. Colorimetric analysis

Visible light reflection spectra in the 400–780 nm range were obtained using a JASCO FP-6500 spectrofluorometer (Tokyo, Japan) equipped with a JEOL ISF-153 integration sphere (Tokyo, Japan). A sample holder (JASCO PSH-001; Tokyo, Japan) was filled with a powdered sample. The reflectance of a Specralon® white standard plate was used for calibration. The reflectance curve was digitalized using a JASCO V-500 color diagnostics program (Tokyo, Japan) and the data were plotted on an L*a*b* color system.

2.4. Ultraviolet (UV) absorption spectrophotometry

UV absorption spectrophotometry was carried out using a JASCO V-600 spectrometer (Tokyo, Japan). The powdered sample was dispersed in ethanol, sonicated for 10 min, and filtered for UV measurement at 320 nm.

2.5. Powder X-ray diffraction (PXRD) measurement

PXRD patterns were obtained using a Rigaku MiniFlex II powder diffractometer (Tokyo, Japan). The X-ray generator was operated at 30 kV and 15 mA using CuKα radiation. The scans were performed between 3° and 35° with a scanning rate of 4°/min at room temperature.

2.6. Thermogravimetry (TG)

TG measurements were operated using a SII Nanotechnology EXSTAR 6000 TG/DTA 6200 (Chiba, Japan). The operating conditions were as follows: platinum open pan; sample weight, ca. 5 mg; heating rate, 5 °C/min; temperature range, 30–800 °C; air flow rate, 200 mL/min.

2.7. Differential scanning calorimetry (DSC)

DSC measurements were performed using SII Nanotechnology EXSTAR6000 DSC6200 (Chiba, Japan). The operating conditions were as follows: crimped-aluminum pan; sample weight, ca. 5 mg; heating rate, 5 °C/min; temperature range, 30–180 °C; nitrogen gas flow rate, 60 mL/min.

2.8. Solid-state ^{13}C NMR spectroscopy

All solid-state ^{13}C NMR measurements were carried out using a JEOL JNM-ECA600 unit (Tokyo, Japan) with a magnetic field of 14.09 T operating at 150 MHz for ^{13}C. Sample powders were placed

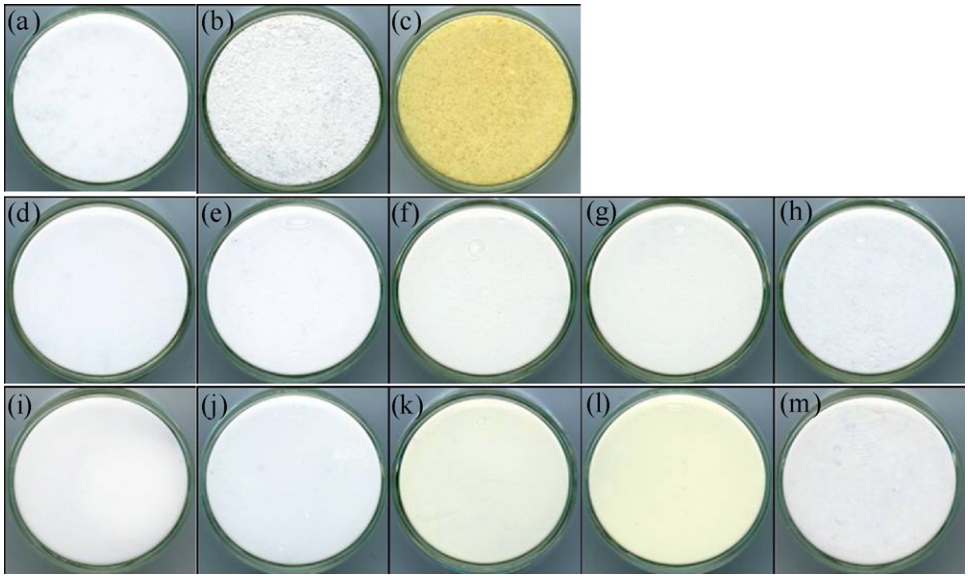

Fig. 2. Sample appearances of (a) γ-IMC, (b) α-IMC, (c) melt-quenched amorphous IMC, (d) TMPS-1.5, (e) IMC/TMPS-1.5 PM 5/5, (f) IMC/TMPS-1.5 EVP 3/7, (g) IMC/TMPS-1.5 EVP 5/5, (h) IMC/TMPS-1.5 EVP 5/5 washed with ethanol, (i) TMPS-7, (j) IMC/TMPS-7 PM 5/5, (k) IMC/TMPS-7 EVP 3/7, (l) IMC/TMPS-7 EVP 5/5, and (m) IMC/TMPS-7 EVP 5/5 washed with ethanol.

into 4-mm silicon nitride (Si_3N_4) rotors. The ^{13}C-pulse saturation transfer and magic angle spinning (PST/MAS) NMR measurements were carried out under the following conditions: sample weight, ca. 100 mg; spinning rate, 18 kHz; relaxation delay, 5 s; number of data points, 2048; integration times, 1000–12,000. All spectra were externally referenced to tetramethylsilane by setting the methyl signal of hexamethylbenzene to 17.3 ppm. Saturation recovery ^{13}C-T_1 measurements with the PST technique were performed under the following conditions: saturation recovery time, 1–100 s; integration times, 200–2000.

3. Results and discussion

3.1. Coloration phenomena

Fig. 2 illustrates the appearances of each sample. Crystalline IMCs (Fig. 2a and b) were white, while melt-quenched amorphous IMC (Fig. 2c) was deep yellow. TMPS-1.5 with a smaller pore size (Fig. 2d) and PM (Fig. 2e) were white. EVP 3/7 (Fig. 2f) and EVP 5/5 (Fig. 2g) of TMPS-1.5 were faint yellow, regardless of the amount of loaded IMC. White color was observed in TMPS-7 with a large pore size (Fig. 2i) and PM (Fig. 2j). In contrast, the EVPs of IMC/TMPS-7 were yellow; the yellow coloration become more yellowish when the weight ratio of IMC to TMPS-7 increased from 3/7 (Fig. 2k) to 5/5 (Fig. 2l).

Visible light absorption and emission can determine the color of samples. To evaluate observed coloration, colorimetric analyses were carried out by visible light reflection spectroscopy (Fig. 3). In Fig. 3a, γ-IMC and α-IMC exhibited high reflectance values in their observed wavelengths, although a slight decrease was observed from 400–420 nm. Melt-quenched amorphous IMC exhibited a significant decrease in visible light in the 400–480 nm range, which corresponds to the violet to blue light region, as well as a small decrease in the 480–570 nm range, which corresponds to the green light region. The deep yellow coloration of melt-quenched amorphous IMC could be due to the absorption of visible light. Melt-quenched amorphous IMC absorbed violet to blue light and resulted in a yellow coloration because yellow is the complementary color of violet to blue. Melt-quenched amorphous IMC also slightly absorbed green light to cause a weak magenta coloration, since magenta is the complementary color of green. The deep yellow color of melt-quenched amorphous IMC was presumably the superimposition of the yellow and magenta coloration. TMPS-1.5, with a smaller pore size (Fig. 3b), constantly reflected visible light. The PM of IMC/TMPS-1.5 exhibited a slight decrease in reflection at 400–420 nm similar to crystalline IMC. In IMC/TMPS-1.5 EVP 3/7 and MC/TMPS-1.5 EVP 5/5, the decrease in reflection at 400–420 nm was greater than that of the PM. The large-pored TMPS-7 and the PM in Fig. 3c demonstrated spectra similar to those of TMPS-1.5 and

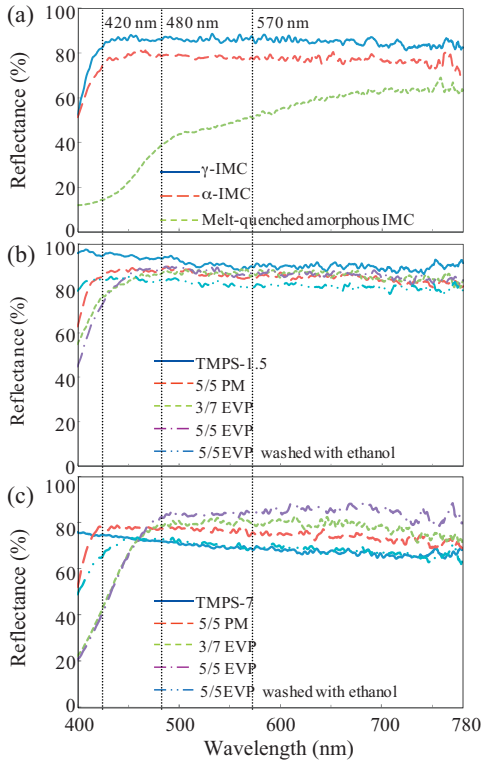

Fig. 3. Reflection spectra of (a) intact IMC, (b) IMC/TMPS-1.5, and (c) IMC/TMPS-7 systems.

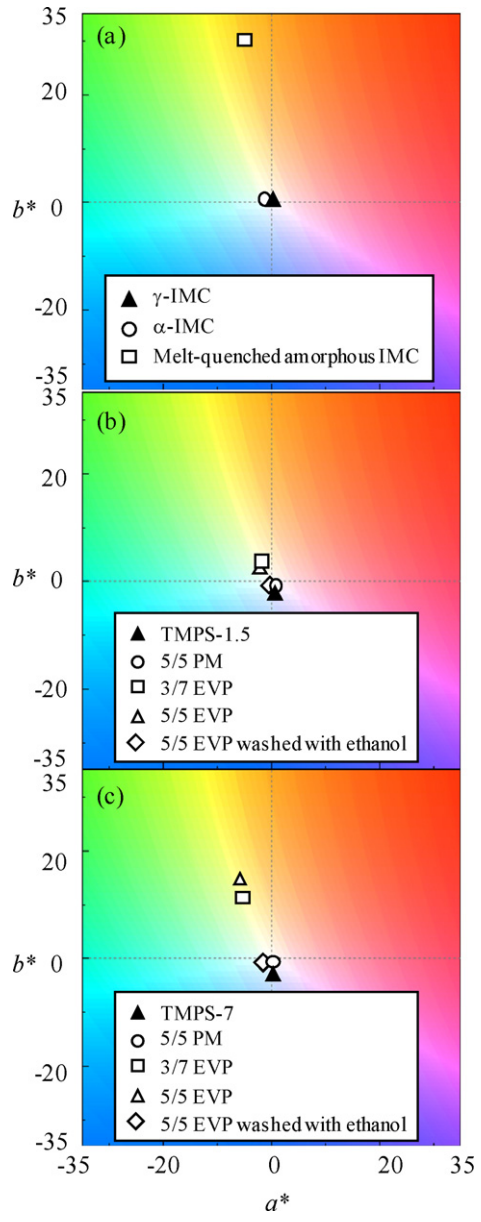

Fig. 4. Colorimetric coordinates of (a) intact IMC, (b) IMC/TMPS-1.5, and (c) IMC/TMPS-7 systems.

the PM in Fig. 3b, respectively. The EVPs of IMC/TMPS-7 exhibited a decrease in reflection at 400–480 nm similar to that of melt-quenched amorphous IMC. However, no significant decrease in reflection at 480–570 nm was observed, which differs from melt-quenched amorphous IMC. This result confirms that the color of IMC/TMPS-7 EVPs is induced by the absorption of violet to blue light, producing yellow. The change in the reflection spectrum of EVP 5/5 was clearly greater than that of EVP 3/7, suggesting that the amount of loaded IMC affects the strength of coloration.

Colorimetric coordinates were calculated from visible light reflection spectra to compare the coloration of each sample in detail; the results were plotted on a three-dimensional color space (Fig. 4). The IMC crystals (Fig. 4a) were positioned around the origin, meaning that IMC was colorless. On the other hand, melt-quenched amorphous IMC had a deep yellow hue. No changes in position were observed for TMPS-1.5 or the PM (Fig. 4b), while the IMC/TMPS-1.5 EVPs exhibited small changes in their positions toward yellow. The positions of TMPS-7 and the PM were almost around the origin (Fig. 4c). In contrast, the positions of IMC/TMPS-7 EVPs indicated a yellow hue, indicating visible light reflection. The position shift from the origin on the a*/b* plane was larger in EVP 5/5 than in EVP 3/7. These results confirm that the loaded amount of IMC can affect the coloration of EVP. It should be noted that melt-quenched amorphous IMC had a different angle from IMC/TMPS-7 EVP on the a*/b* plane, indicating a difference in their color.

Table 1
IMC (%) dissolved into ethanol from EVP.

Sample	Dissolved IMC (%)
IMC/TMPS-1.5 EVP 5/5	94.0 ± 0.9
IMC/TMPS-7 EVP 5/5	93.2 ± 1.0

(n = 3, mean ± SD)

3.2. Coloration reversibility

To evaluate the reversibility of the EVPs' yellow coloration, IMC/TMPS-1.5 EVP 5/5 and IMC/TMPS-7 EVP 5/5 were dispersed in ethanol, and the amount of dissolved IMC was determined. Quantitative UV measurement confirmed that nearly 95% of loaded IMC was eluted from both EVPs by ethanol (Table 1). IMC (5%) could remain in the TMPS pores. TG measurement showed that 1–3% of water and ethanol existed in the EVPs (data not shown), suggesting that the amount of eluted IMC was an underestimate. These results indicate that almost all loaded IMC can be washed out by ethanol. EVPs washed out by ethanol exhibited white color, as shown in Fig. 2h and m; moreover, their colorimetric coordinates were close to the origin, corresponding to pure TMPS (Fig. 4). The ^{1}H NMR spectrum from the eluting solvent (d-chloroform) of the EVP was identical to that from intact IMC and showed no peak derived from IMC decomposition (data not shown). Therefore, it can be concluded that the yellow coloration of the EVP was resulted from the changes in molecular state of IMC incorporated into TMPS, not the decomposition or chemical reaction of IMC.

3.3. PXRD measurement

PXRD measurement was carried out to investigate the incorporation of IMC into TMPS mesopores (Fig. 5). Characteristic peaks were observed for γ-IMC (Fig. 5a) at 2θ = 11.6°, 19.6°, 21.9°, 26.6°, and 29.1°; those for α-IMC (Fig. 5b) were at 2θ = 8.4°, 11.9°, 14.4°, 18.0°, and 22.1°. The peak positions of IMC crystals were consistent with those in a previous report (Masuda et al., 2006). Melt-quenched amorphous IMC exhibited a halo pattern without characteristic IMC peaks (Fig. 5c). The PMs containing TMPS-1.5 and TMPS-7 (Fig. 5d and g) demonstrated distinct peaks belonging to γ-IMC (Fig. 5a), indicating the existence of γ-IMC crystal in the mixture. The diffraction patterns of IMC/TMPS-1.5 EVPs (Fig. 5e and f) showed peaks corresponding to α-IMC crystals. Meanwhile, IMC/TMPS-7 EVPs (Fig. 5h and i) showed PXRD halo patterns regardless of the different loaded weight ratios of IMC to TMPS-7; no peaks derived from crystalline γ-IMC/α-IMC were observed either. γ-IMC turned to α-IMC via evaporation when ethanol was used as a solvent (data not shown). The PXRD results indicate that TMPS-7 with a larger pore size can entrap almost all IMC, although a little IMC is incorporated into the pores of TMPS-1.5 with smaller pores. Incorporation of IMC into the pores changes its molecular state from crystalline to amorphous.

3.4. DSC analysis

The relationship between coloration and the amount of amorphous IMC in the mesopores was investigated by DSC measurement (Fig. 6) and quantitative analysis (Fig. 7). γ-IMC and α-IMC showed melting peaks at 161 °C and 152 °C, respectively. The DSC curves of

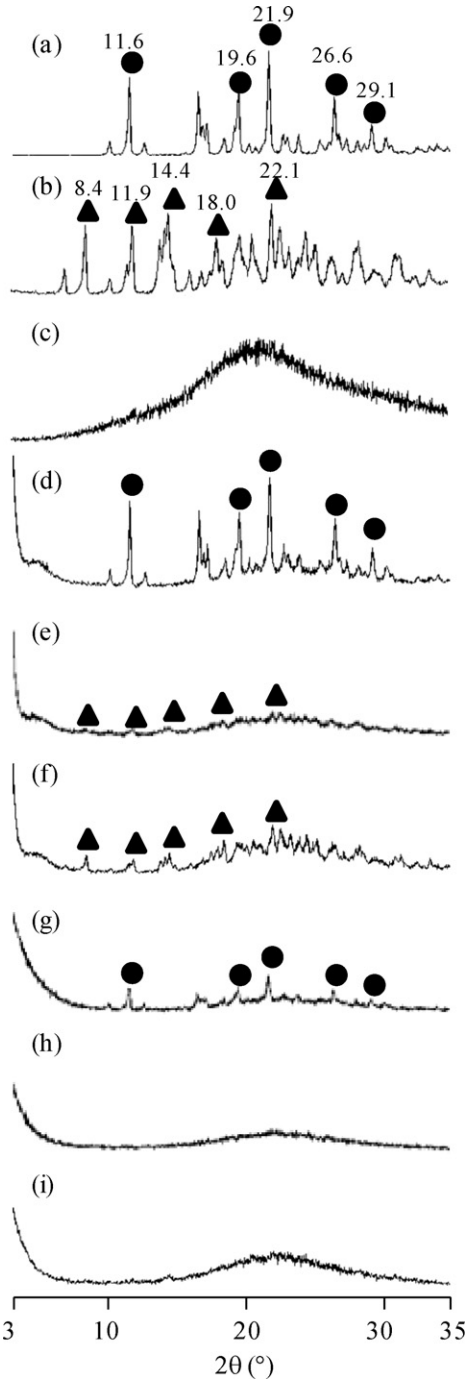

Fig. 5. PXRD patterns of (a) γ-IMC, (b) α-IMC, (c) melt-quenched amorphous IMC, (d) IMC/TMPS-1.5 PM 5/5, (e) IMC/TMPS-1.5 EVP 3/7, (f) IMC/TMPS-1.5 EVP 5/5, (g) IMC/TMPS-7 PM 5/5, (h) IMC/TMPS-7 EVP 3/7, and (i) IMC/TMPS-7 EVP 5/5.

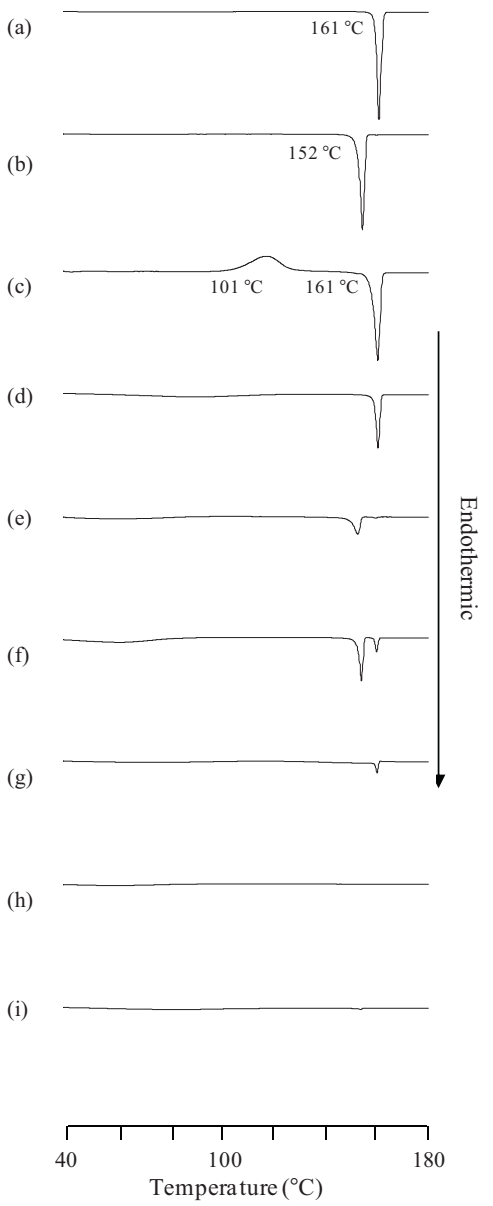

Fig. 6. DSC curves of (a) γ-IMC, (b) α-IMC, (c) melt-quenched amorphous IMC, (d) IMC/TMPS-1.5 PM 5/5, (e) IMC/TMPS-1.5 EVP 3/7, (f) IMC/TMPS-1.5 EVP 5/5, (g) IMC/TMPS-7 PM 5/5, (h) IMC/TMPS-7 EVP 3/7, (i) IMC/TMPS-7 EVP 5/5.

melt-quenched amorphous IMC (Fig. 6c) denoting crystallization at 101 °C and melting of γ-IMC. PMs (Fig. 6d and g) indicated the melting peak of γ-IMC, demonstrating the existence of γ-IMC crystals, which is concordant with the PXRD results. IMC/TMPS-1.5 EVP 3/7 and IMC/TMPS-1.5 EVP 5/5 showed melting peaks of both γ-IMC and α-IMC in the DSC curves (Fig. 6e and f). On the other hand, IMC/TMPS-7 EVP 3/7 and IMC/TMPS-7 EVP 5/5 EVP showed no peaks derived from the crystallization or melting of IMC (Fig. 6h and i). It is reported that the inclusion of organic guest molecules into mesopores inhibits the crystallization of guest molecules (Azaïs et al., 2006; Speybroeck et al., 2009). IMC/TMPS-7 EVPs lacking crystallization behavior indicate that most amorphous IMC molecules were stabilized in the mesopores even during the heating process and that the molecular state of amorphous IMC inside the pores should be different from that of melt-quenched amorphous IMC.

The weight percent of γ-IMC, α-IMC, and amorphous IMC in the EVPs were calculated from the melting enthalpy (ΔH) of IMC in the DSC curves (Fig. 7). Since the amount of amorphous IMC to sum of IMC and TMPS in IMC/TMPS-1.5 EVPs 3/7 and 5/5 was only 3.4% and 4.8%, respectively; most IMC in IMC/TMPS-1.5 EVPs existed in crystalline state. However, most IMC in IMC/TMPS-7 EVP 3/7 and 5/5 was in an amorphous state. Quantitative analysis from the DSC curves revealed that the amount of amorphous IMC in IMC/TMPS-7 was significantly higher than that in IMC/TMPS-1.5. It was speculated that the relationship between the molecular state of IMC and coloration mechanism as follows. For a slightly yellow sample of IMC/TMPS-1.5 EVP, IMC was not incorporated into the mesopores due to the smaller mesopore size. Most IMC molecules should exist in a crystalline state, although a little amorphous IMC was possibly on the outer surface of the TMPS pores. In a yellow

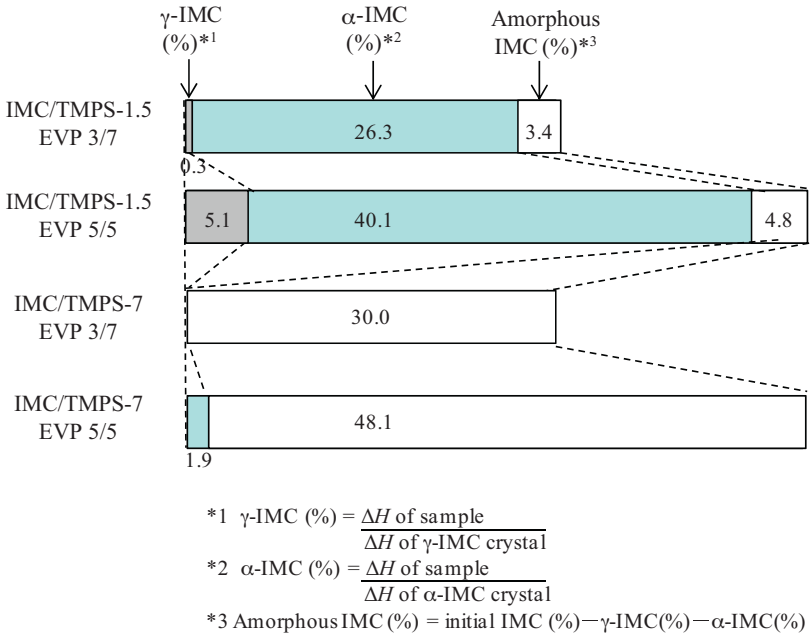

Fig. 7. Amount of IMC (%) in each EVP calculated from DSC curves ($n = 3$).

sample of IMC/TMPS-7 EVP, most IMC was incorporated into the large mesopores in an amorphous state. The amount of incorporated amorphous IMC could be related to the yellow coloration since IMC/TMPS-7 EVP 5/5 exhibited a brilliant yellow color compared to IMC/TMPS-7 EVP 3/7.

3.5. Solid-state ^{13}C NMR measurement

To determine the coloration mechanism, the molecular state of IMC inside the mesopores was evaluated by solid-state ^{13}C-PST/MAS NMR (Fig. 8). The ^{13}C-PST/MAS NMR method can detect relatively high mobility groups/molecules (Moribe et al., 2010). The peak assignments of each carbon derived from γ-IMC, α-IMC, and melt-quenched amorphous IMC were corroborated by those in a previous report (Masuda et al., 2006). The numbering of carbon atoms is shown in Fig. 1. γ-IMC exhibited sharp peaks for methyl (C13) and methoxy (C12) carbons. α-IMC showed weak peaks for carboxyl (C11) and aromatic (C1′, 2′, 3′, 4′, 2, 8, and 9) carbons in addition to sharp peaks for methyl and methoxy carbons. The carboxyl and aromatic carbons of α-IMC were more distinct than that of γ-IMC, presumably due to the higher mobility of α-IMC. Melt-quenched amorphous IMC showed sharp methylene (C10) and weak amide carbonyl (C14) carbon peaks in addition to peaks for crystalline γ-IMC and α-IMC. The peak intensities of aromatic carbons (C1′, 2′, 3′, 4′, 2, 8, 9, 3, 7, 6, and 4) in melt-quenched amorphous IMC were much higher than those in crystalline IMC. Melt-quenched amorphous IMC had high mobility in the aromatic, amide carbonyl, methylene, and carboxylic carbons.

IMC/TMPS-1.5 EVP 5/5 demonstrated almost the same spectrum as that of α-IMC, which is concordant with the DSC results. Conversely, both IMC/TMPS-7 EVP 3/7 and 5/5 showed intensive peaks of aromatic, methoxy, methylene, and methyl carbons in the spectra similar to melt-quenched amorphous IMC. However, the relative peak intensities of aromatic carbons compared to methyl and methoxy carbons were remarkably different from those of melt-quenched amorphous IMC. These results indicate that the local mobility of IMC in TMPS-7 pores is different from that of melt-quenched amorphous IMC (Pham et al., 2010).

The ^{13}C spin–lattice relaxation (^{13}C-T_1) measurements were performed to assess the local molecular mobility of melt-quenched amorphous IMC and IMC incorporated into the pores of TMPS-7 (Table 2). All ^{13}C-T_1 values obtained at 35 °C were smaller than those obtained at 25 °C. Since molecules at high temperatures should exhibit faster motion, both the motion of melt-quenched amorphous IMC and IMC in the pores of TMPS-7 at 25 °C and 35 °C should be on the slow motional side of the T_1 minimum (Tseng et al., 1997). In melt-quenched amorphous IMC, the aromatic groups, including indole and phenyl rings, demonstrated much longer ^{13}C-T_1 values (>10 times) than side chains. These results are consistent with those of a previous report (Masuda et al., 2006), in which the aromatic rings of melt-quenched amorphous IMC under a T_g of approximately 40 °C demonstrated substantially restricted molecular mobility while the side chains, having free rotation, had faster local mobility. Similarly, the ^{13}C-T_1 of IMC in TMPS-7 was longer in the aromatic groups than in the side chains. However, the variations in ^{13}C-T_1 between the aromatic groups and side chains of IMC in TMPS-7 were small (ca. 2–3 times); this means that the aromatic carbons of IMC in TMPS-7 are free and their mobility is different from those of melt-quenched amorphous IMC. Furthermore, this suggests that IMC has entirely faster dynamics in the limited spaces of TMPS mesopores.

3.6. Speculated coloration mechanism

The yellow coloration of IMC observed in this study could be due to the red shift of the absorption band from the ultraviolet

Table 2
^{13}C-T_1 of IMC in melt-quenched amorphous IMC and IMC/TMPS-7 EVP 3/7.

^{13}C	^{13}C-T_1 (s)			
	Melt-quenched amorphous IMC		IMC/TMPS-7 EVP 3/7	
	25 °C	35 °C	25 °C	35 °C
13	3.7	2.2	2.6	1.7
12	3.7	3.0	2.5	2.0
3,6,7,4	59.0	39.2	4.5	2.9
1′,2′,3′,4′,2,8,9	40.3	38.2	5.4	4.8

The ^{13}C-T_1 of C5, 10, 11 and 14 did not fit the least squares fitting due to low peak intensity.

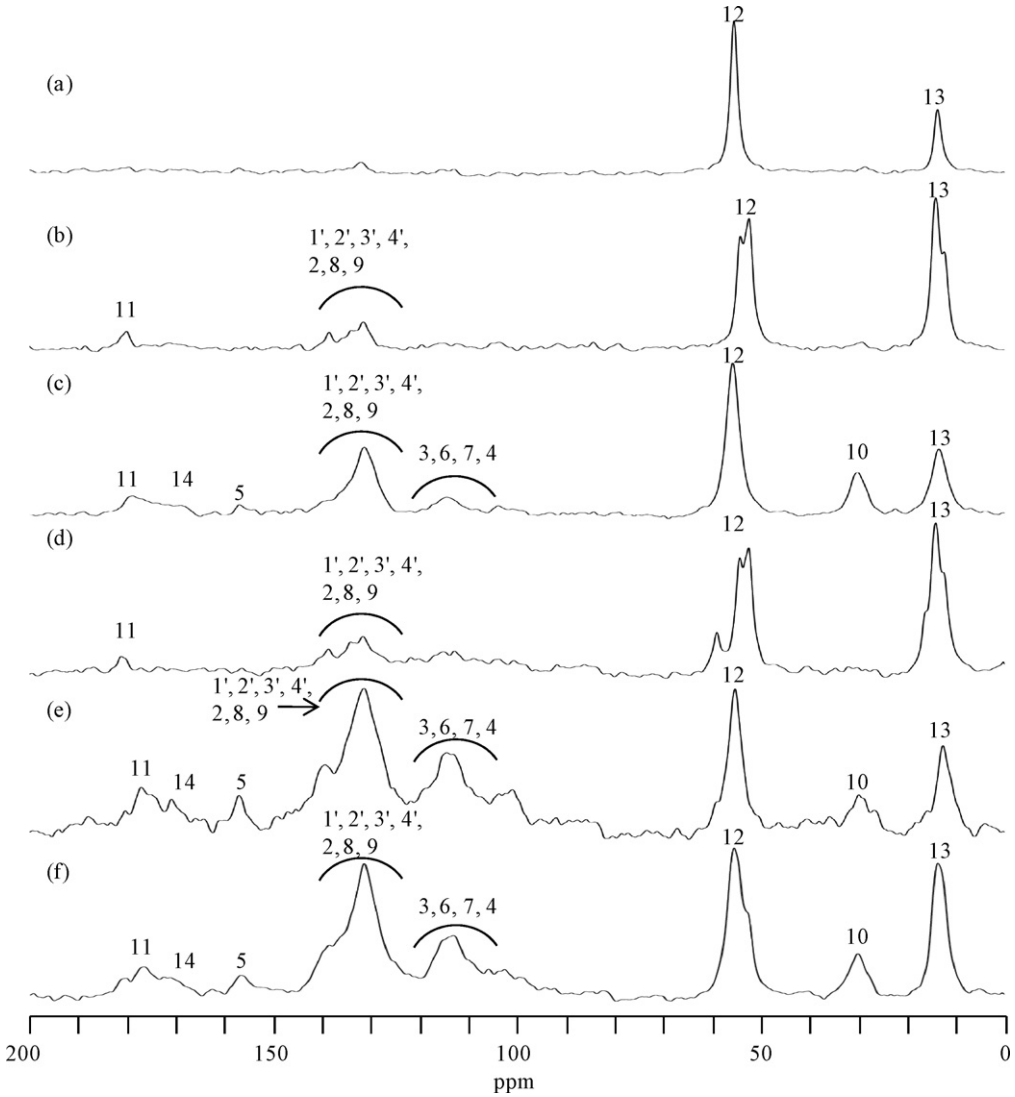

Fig. 8. ^{13}C-PST/MAS spectra of (a) γ-IMC, (b) α-IMC, (c) melt-quenched amorphous IMC, (d) IMC/TMPS-1.5 EVP 5/5, (e) IMC/TMPS-7 EVP 3/7, and (f) IMC/TMPS-7 EVP 5/5.

region to the visible light region, which is supported by the results shown in Fig. 3. The chemical structure of IMC contains two π-conjugated rings: indole and benzene (Fig. 9). The indole ring has the following electron donors: methyl, methoxy, and methylene groups, while the benzene ring has a chloride atom as an electron donor. An electron-attractive keto group connects these rings, and possibly conjugates with the indole and benzene rings. However, all π-conjugation systems are on different planes in the crystal structure, thereby forcing the separated local π-conjugation systems (Li and Feng, 2005). Due to the non-planar structure of IMC crystals, π-conjugation should not be extended as shown in Fig. 9a. The constraint of non-planar structure in both melt-quenched amorphous IMC and amorphous IMC in the pores of TMPS-7 could be reduced compared to crystal IMC. Thus, these samples exhibited coloration due to the n–π* or π–π* transition that emerged because of the extended π-conjugation systems. The possible intramolecular extended π-conjugation systems of IMC are shown in Fig. 9b–d. In the ^{13}C-PST/MAS NMR spectra of crystal and melt-quenched amorphous IMCs, a difference in the peak intensity of the aromatic ring is clearly observable. The changes in the molecular state from

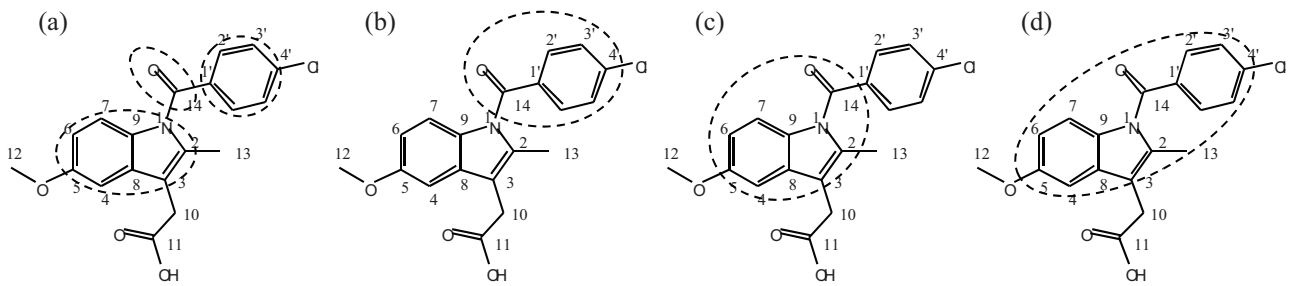

Fig. 9. Possible intramolecular π-conjugation systems in an IMC molecule.

crystal to amorphous should lead to the yellow coloration due to the formation of an extended π-conjugation system (Sheth et al., 2005; Braun et al., 2008). This suggestion is also supported by the fact that dissolved IMC is yellow in organic solvents that are in a monomolecular state such as ethanol (data not shown).

The color difference between melt-quenched amorphous IMC and amorphous IMC in the pores of TMPS-7 was discussed. The reflection spectrum of melt-quenched amorphous IMC (Fig. 3) exhibited two absorption bands that could be derived from the different extended π-conjugation systems proposed in Fig. 9b–d. In contrast, amorphous IMC in the pores of TMPS-7 only showed a single absorption band in the reflection spectrum (Fig. 3), which could be derived from one of the extended π-conjugation systems. The ^{13}C-PST/MAS NMR and ^{13}C-T_1 measurements showed that the mobility of melt-quenched amorphous IMC and amorphous IMC in the pores of TMPS-7, especially around the aromatic rings, are very different. The confined environment in the mesopores should lead to a flexible conformation of IMC. In contrast, melt-quenched amorphous IMC has different extended π-conjugation systems. Though direct evaluation was not performed, intermolecular interaction between IMC and TMPS could exist on the surface of TMPS mesopore. Yellow coloration of IMC/TMPS EVP could result from the intermolecular interaction between IMC and TMPS in addition to amorphization of IMC molecule. This suggestion was supported by the similar but not identical ^{13}C-PST/MAS NMR spectra, relaxation time, and kind of color of incorporated IMC and melt-quenched IMC.

4. Conclusions

This study evaluated the yellow coloration phenomena of IMC both qualitatively and quantitatively by colorimetric analysis, PXRD, DSC, and solid-state NMR. The results show that amorphous IMC incorporated into the pores of TMPS-7 via evaporation causes the yellow coloration. The difference in color brilliance between the samples can be explained by the amount of amorphous IMC. Furthermore, the differences in the intramolecular π-conjugation systems of aromatic rings could produce the color difference between IMC/TMPS-7 EVP and melt-quenched amorphous IMC. The knowledge acquired from this study is expected to help our understanding of coloration mechanisms that are often observed in solid formulation studies.

Acknowledgments

We would like to thank Taiyo Kagaku Co., Ltd. for kind provision of TMPS. NMR experiments were supported by Chemical Analysis Center, Chiba University. This study was supported by a Grant-in-Aid for Scientific Research from the Ministry of Education, Culture, Sports, Science and Technology (Monbukagakusho), Japan (21790032, 21590038), Japan Health Sciences Foundation for Research on Publicly Essential Drugs, and Medical Devices, and OTC Self-Medication Promotion Foundation (Sato Pharmaceutical Co., Ltd.).

References

Ambrogi, V., Perioli, L., Marmottini, F., Giovagnoli, S., Esposito, M., Rossi, C., 2007. Improvement of dissolution rate of piroxicam by inclusion into MCM-41 mesoporous silicate. Eur. J. Pharm. Sci. 32, 216–222.

Azaïs, T., Tourné-Péteilh, C., Aussenac, F., Baccile, N., Coelho, C., Devoisselle, J.M., Babonneau, F., 2006. Solid-state NMR study of Ibuprofen confined in MCM-41 material. Chem. Mater. 18, 6382–6390.

Braun, D.E., Gelbrich, T., Jetti, R.K.R., Kahlenberg, V., Price, S.L., Griesser, U.J., 2008. Colored polymorphs: thermochemical and structural features of N-picryl-p-toluidine polymorphs and solvates. Cryst. Growth Des. 8, 1977–1989.

Geppi, M., Mollica, G., Borsacchi, S., Veracini, C.A., 2008. Solid-state NMR studies of pharmaceutical systems. Appl. Spectrosc. Rev. 43, 202–302.

Komori, Y., Hayashi, S., 2003. Reversible change in optical properties of chromophores in zeolites by interaction with alkali metal cations. Chem. Mater. 15, 4598–4603.

Komori, Y., Hayashi, S., 2004. Effects of Na^+ on dynamics of p-nitroaniline molecules in zeolite ZSM-5 studied by solid-state NMR. Bull. Chem. Soc. Jpn. 77, 673–679.

Li, T., Feng, S., 2005. Study of crystal packing on the solid-state reactivity of indomethacin with density functional theory. Pharm. Res. 22 (11), 1964–1969.

Lubach, J.W., Xu, D., Segmuller, B.E., Munson, E.J., 2007. Investigation of the effects of pharmaceutical processing upon solid-state NMR relaxation times and implications to solid-state formulation stability. J. Pharm. Sci. 96, 777–787.

Masuda, K., Tabata, S., Kono, H., Sakata, Y., Hayase, T., Yonemochi, E., Terada, K., 2006. Solid-state ^{13}C NMR study of indomethacin polymorphism. Int. J. Pharm. 318, 146–153.

Mellaerts, R., Mols, R., Jammaer, J.A.G., Aerts, C.A., Annaert, P., Humbeeck, J.V., Mooter, G.V., Augustijns, P., Martens, J.A., 2008. Increasing the oral bioavailability of the poorly water soluble drug itraconazole with ordered mesoporous silica. Eur. J. Pharm. Biopharm. 69, 223–230.

Moribe, K., Kinoshita, R., Higashi, K., Tozuka, Y., Yamamoto, K., 2010. Coloration phenomenon of mefenamic acid in mesoporous silica FSM-16. Chem. Pharm. Bull. 58, 214–218.

Morimoto, M., Kobatake, S., Irie, M., 2003. Multicolor photochromism of two- and three-component diarylethene crystals. J. Am. Chem. Soc. 125, 11080–11087.

Nishiwaki, A., Watanabe, A., Higashi, K., Tozuka, Y., Moribe, K., Yamamoto, K., 2009. Molecular states of prednisolone dispersed in folded sheet mesoporous silica (FSM-16). Int. J. Pharm. 378, 17–22.

Pham, T.N., Watson, S.A., Edwards, A.J., Chavda, M., Clawson, J.S., Strohmeier, M., Vogt, F.G., 2010. Analysis of amorphous solid dispersions using 2D solid-state NMR and 1H T1 relaxation measurements. Mol. Pharm. 7, 1667–1691.

Rhee, Y.-S., Park, C.-W., Shin, Y.-S., Kam, S.-H., Lee, K.-H., Park, E.-S., 2008. Application of instrumental evaluation of color for the pre-formulation and formulation of rabeprazole. Int. J. Pharm. 350, 122–129.

Savolainen, M., Heinz, A., Strachan, C., Gordon, K.C., Yliruusi, J., Rades, T., Sandler, N., 2007. Screening for differences in the amorphous state of indomethacin using multivariate visualization. Eur. J. Pharm. Sci. 30, 113–123.

Shen, P., Liu, Y., Huang, X., Zhao, B., Xiang, N., Fei, J., Liu, L., Wang, X., Huang, H., Tan, S., 2009. Efficient triphenylamine dyes for solar cells: effects of alkyl-substituents and π-conjugated thiophene unit. Dye Pig. 83, 187–197.

Sheth, A.R., Lubach, J.W., Munson, E.J., Muller, F.X., Grant, D.J.W., 2005. Mechanochromism of piroxicam accompanied by intermolecular proton transfer probed by spectroscopic methods and solid-phase changes. J. Am. Chem. Soc. 127, 6641–6651.

Siddiqui, A., Nazzal, S., 2007. Measurement of surface color as an expedient QC method for the detection of deviations in tablet hardness. Int. J. Pharm. 341, 173–180.

Siewertsen, R., Neumann, H., Buchheim-Stehn, B., Herges, R., Näther, C., Renth, F., Temps, F., 2009. Highly efficient reversible Z-E photoisomerization of a bridged azobenzene with visible light through resolved $S_1(n\pi^*)$ absorption bands. J. Am. Chem. Soc. 131, 15594–15595.

Speybroeck, M.V., Barillaro, V., Thi, T.D., Mellaerts, R., Martens, J., Humbeeck, J.V., Vermant, J., Annaert, P., Mooter, G.V.D., Augustijns, P., 2009. Ordered mesoporous silica material SBA-15: a broad-spectrum formulation platform for poorly soluble drugs. J. Pharm. Sci. 98, 2648–2658.

Tishmack, P.A., Bugay, D.E., Byrn, S.R., 2003. Solid-state nuclear magnetic resonance spectroscopy-pharmaceutical applications. J. Pharm. Sci. 92, 441–474.

Tozuka, Y., Oguchi, T., Yamamoto, K., 2003. Adsorption and entrapment of salicylamide molecules into the mesoporous structure of folded sheets mesoporous material (FSM-16). Pharm. Res. 20, 926–930.

Tozuka, Y., Wongmekiat, A., Kimura, K., Moribe, K., Yamamoto, K., 2005a. Effect of pore size of FSM-16 on the entrapment of flurbiprofen in mesoporous structure. Chem. Pharm. Bull. 53, 974–977.

Tozuka, Y., Sasaoka, S., Nagae, A., Moribe, K., Oguchi, T., Yamamoto, K., 2005b. Rapid adsorption and entrapment of benzoic acid molecules onto mesoporous silica (FSM-16). J. Colloid Interface Sci. 291, 471–476.

Tseng, W.-Y., Chen, Y.-H., Khairullin, I.I., Cheng, S., Hwang, L.-P., 1997. NMR study of solid C60 (γ-cyclodextrin) 2. Solid State Nucl. Magn. Reson. 8, 219–229.

Yamamura, M., Kano, N., Kawashima, T., Matsumoto, T., Harada, J., Ogawa, K., 2008. Crucial role of N···Si interactions in the solid-state coloration of disilylazobenzenes. J. Org. Chem. 73, 8244–8249.